Regenerative Dynamometer with Vector Controlled Drive

Dipankar De and V Ramanarayanan
Department of Electrical Engineering,
Indian Institute of Science, Bangalore, India

***Abstract*— This paper presents the topology selection, design steps, simulation studies, design verification, system fabrication and performance evaluation on an induction motor based dynamometer system. The control algorithm used the application is well known field oriented control or vector control. Position sensorless scheme is adopted to eliminate the encoder requirement. The dynamometer is rated for 3.7kW. It can be used to determine the speed–torque characteristics of any rotating system. The rotating system is to be coupled with the vector controlled drive and the required torque command is given from the latter. The experimental verification is carried out for an open loop v/f drive as a test rotating system and important test results are presented.**

***Index Terms*— AC motor drives, Vector control, Dynamometer, Four quadrant operation, Position sensorless, Hysteresis control.**

I. Introduction

There are a number of legacy application of dynamometer for evaluating the torque–speed characteristics of any rotating system like electric machines, diesel engine etc. Conventionally, DC drive is widely used for this application because of its simple control strategies. But DC machine requires frequent maintenance due to the presence of commutators and brushes. Hence, DC machine can be replaced by rugged and maintenance free induction machine, but at the cost of complex control [1], [2]. This paper describes the application of induction machine as a dynamometer.

II. System Architecture

A typical dynamometer system is shown in fig–1. The rotating system is coupled to the rotor of a specially designed induction machine. The stator of this machine is free to move, but the movement is restricted by a load cell (torque transducer). The rotating device employed in the present work is a v/f drive system. The v/f drive coupled to vector controlled drive is shown in fig–2. The input is taken from 3Φ $415V$ AC source and rectified by the diode bridge rectifier in order to get DC bus of $586V$. In this configuration two separate rectifier–inverter set are used for two separate machines. The braking resistor (BR) across the dc bus of vector controlled drive is essential for a non-electrical rotating system. In case of v/f drive system, the DC bus of both the drive are made common in order to eliminate braking resistor and associated losses [3]. This configuration also enables four-quadrant operation of the drive system (fig–3). Input side line inductors are added to reduce peaky rectifier current drawn from the grid.

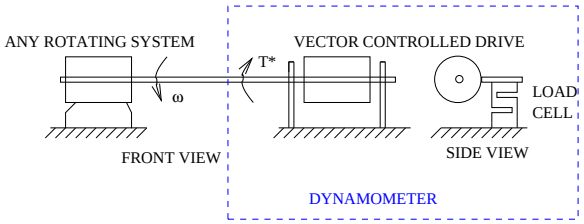

Fig. 1: Mechanical arrangement

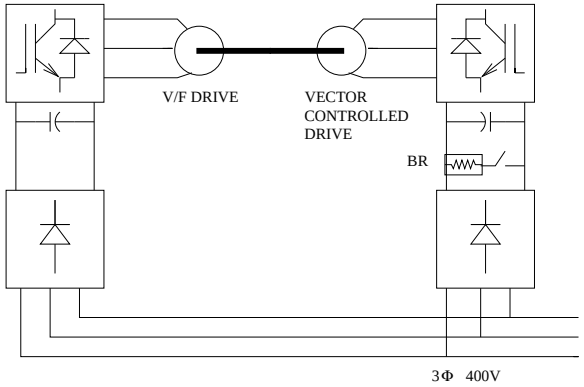

Fig. 2: Power Circuit Diagram of dynamometer

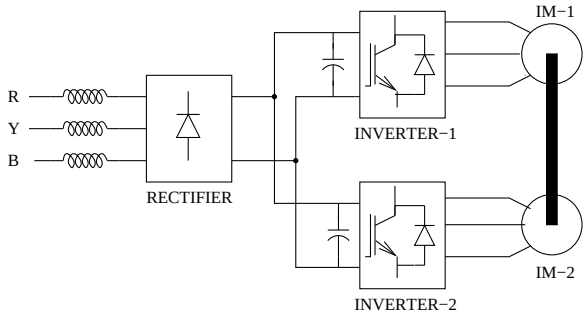

Fig. 3: Modified Power Circuit Diagram of dynamometer

III. Position Sensorless Vector Control

The concept of viewing AC machine analogous to DC machine by changing the frame of reference is known as vector control or field oriented control. In the present scheme position sensorless control is adopted. A speed encoder is undesirable in a drive system because it adds to costs and reliability problems, besides the need for a shaft extensionand

mounting arrangements [5]. The estimation process is shown in fig–4. The overall control algorithm is subdivided in four subsections as follows.

- Unit vector generation ($cos\rho$ and $sin\rho$)
- Estimation of ω_{mr} and ω
- Control loops
- Feed–forward terms

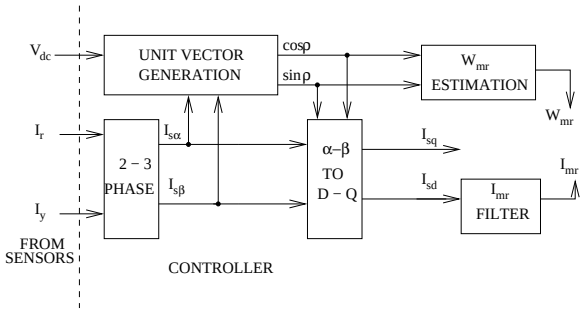

Fig. 4: Derivation of important signals

The three feedback signals from sensor (R-phase line current, Y-phase line current and DC bus voltage) are processed to get desired control signal and direction of unit vector. The direction of d-axis is taken along the rotor flux because of natural decoupling of d and q axis quantities.

A. Unit vector generation

The vector control is basically the current control of the machine. We split the stator current vector in two parts – flux producing component or reactive component along rotor flux (d -axis) and torque producing component or active component in a direction perpendicular to rotor flux. The generation of unit vector is basically to identify the position of rotor flux (fig–5). The stator fluxes (α and β component) in stationary coordinate system is derived by integrating respective back e.m.f.s. From $\psi_{s\alpha}$ and $\psi_{s\beta}$, the rotor fluxes $\psi_{r\alpha}$ and $\psi_{r\beta}$ are calculated and scaled to get the unit vectors ($cos\rho$ and $sin\rho$).

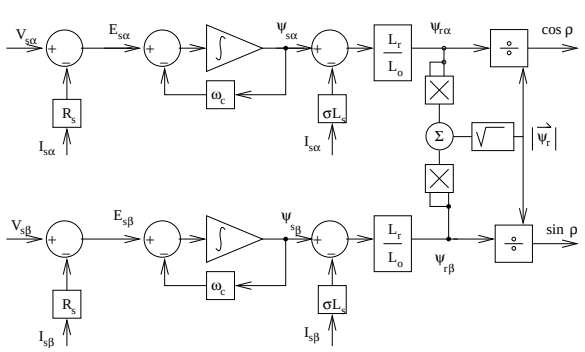

Fig. 5: Unit vector generation

B. Estimation of ω_{mr} and ω

The synchronous speed ω_{mr} is defined as the derivative of ρ. As the continuous signals $sin\rho$ and $cos\rho$ are already available hence ω_{mr} is determined as follows.

$$\omega_{mr} = cos\rho\frac{d(sin\rho)}{dt} - sin\rho\frac{d(cos\rho)}{dt} \quad (1)$$

In order to eliminate the noise associate with the differentiation process a heavy filter is used (fig–6). In present application determination of speed by subtracting $\omega_{slip}$from ω_{mr} is optional.

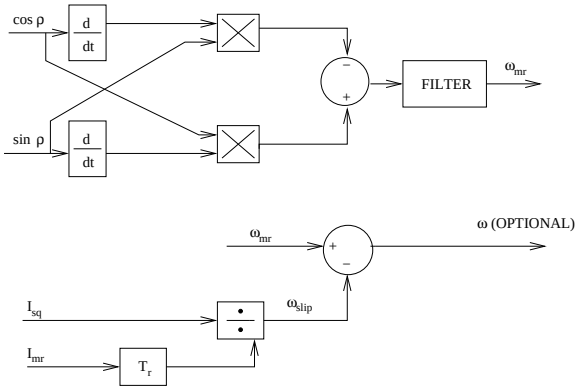

Fig. 6: Evaluation of speed

C. Control loops

The control loop basically consists of d and q axis current control loop and flux loop (fig–7). The flux reference or equivalently i^*_{mr} is compared with derived i_{mr} feedback and error is given to flux controller. The output from the flux controller is d axis current reference. On the other side, q-axis current reference is directly given by the user. The voltage references from the current controller is then combined with feed-forward terms for perfect decoupling. The feedforward block will be discussed in next section. After decoupling, these reference voltages undergo d-q to $\alpha-\beta$ and 2-phase to 3-phase transformation to generate three sinusoidal voltage references for modulator.

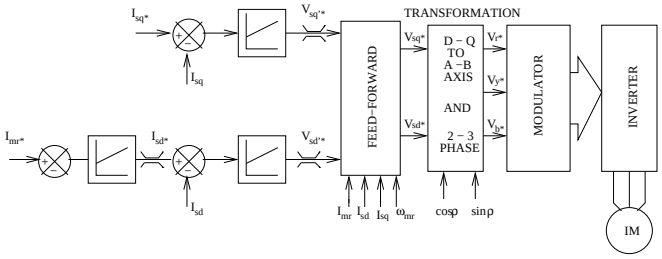

Fig. 7: Control block diagram

D. Feed–forward terms

The feed–forward terms are essential for perfect decoupling. The transformed stator equation to the rotor flux reference frame can be written as

$$V_{sd} = R_s I_{sd} + \sigma L_s \frac{d}{dt} I_{sd} - \omega_{mr}\sigma L_s I_{sq} + (1-\sigma) L_s \frac{d}{dt} I_{mr} \quad (2)$$

$$V_{sq} = R_s I_{sq} + \sigma L_s \frac{d}{dt} I_{sq} + \omega_{mr} \sigma L_s I_{sd} + (1-\sigma)\omega_{mr} L_s I_{mr} \quad (3)$$

Accordingly, the feedforward terms are shown in fig–8

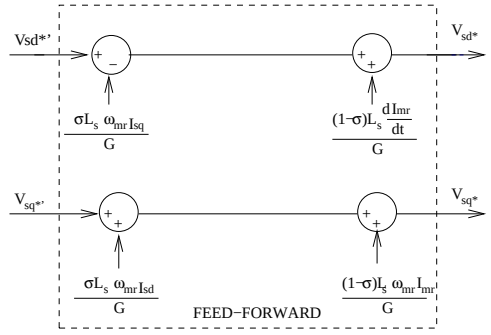

Fig. 8: Feed–forward terms

IV. Modelling and Controller Design

A. Modelling in $\alpha - \beta$ Coordinate Systems

The vector controlled drive coupled with v/f drive shares a common mechanical system. The electrical dynamic equations of both the machines are independent to each other. These dynamic equations are detailed as follows.

$$\begin{aligned}
\sigma_1 T_{s1} \tfrac{di_{s\alpha 1}}{dt} &= \tfrac{1}{R_{s1}} v_{s\alpha 1} - i_{s\alpha 1} + \omega_e T_{s1}(1-\sigma_1) i_{s\beta 1} \\
&\quad + \tfrac{T_{s1}}{T_{r1}(1+\sigma_{s1})} i_{r\alpha 1} + \tfrac{\omega_e T_{s1}}{1+\sigma_{s1}} i_{r\beta 1} \\
\sigma_2 T_{s2} \tfrac{di_{s\alpha 2}}{dt} &= \tfrac{1}{R_{s2}} v_{s\alpha 2} - i_{s\alpha 2} + \omega_e T_{s2}(1-\sigma_2) i_{s\beta 2} \\
&\quad + \tfrac{T_{s2}}{T_{r2}(1+\sigma_{s2})} i_{r\alpha 2} + \tfrac{\omega_e T_{s2}}{1+\sigma_{s2}} i_{r\beta 2} \\
\sigma_1 T_{s1} \tfrac{di_{s\beta 1}}{dt} &= \tfrac{1}{R_{s1}} v_{s\beta 1} - \omega_e T_{s1}(1-\sigma_1) i_{s\alpha 1} - i_{s\beta 1} \\
&\quad - \tfrac{\omega_e T_{s1}}{1+\sigma_{s1}} i_{r\alpha 1} + \tfrac{T_{s1}}{T_{r1}(1+\sigma_{s1})} i_{r\beta 1} \\
\sigma_2 T_{s2} \tfrac{di_{s\beta 2}}{dt} &= \tfrac{1}{R_{s2}} v_{s\beta 2} - \omega_e T_{s2}(1-\sigma_2) i_{s\alpha 2} - i_{s\beta 2} \\
&\quad - \tfrac{\omega_e T_{s2}}{1+\sigma_{s2}} i_{r\alpha 2} + \tfrac{T_{s2}}{T_{r2}(1+\sigma_{s2})} i_{r\beta 2} \\
\sigma_1 T_{r1} \tfrac{di_{r\alpha 1}}{dt} &= \tfrac{-1}{R_{r1}(1+\sigma_{s1})} v_{s\alpha 1} + \tfrac{T_{r1}}{T_{s1}(1+\sigma_{r1})} i_{s\alpha 1} \\
&\quad - \tfrac{\omega_e T_{r1}}{1+\sigma_{r1}} i_{s\beta 1} - i_{r\alpha 1} - \omega_e T_{r1} i_{r\beta 1} \\
\sigma_2 T_{r2} \tfrac{di_{r\alpha 2}}{dt} &= \tfrac{-1}{R_{r2}(1+\sigma_{s2})} v_{s\alpha 2} + \tfrac{T_{r2}}{T_{s2}(1+\sigma_{r2})} i_{s\alpha 2} \\
&\quad - \tfrac{\omega_e T_{r2}}{1+\sigma_{r2}} i_{s\beta 2} - i_{r\alpha 2} - \omega_e T_{r2} i_{r\beta 2} \\
\sigma_1 T_{r1} \tfrac{di_{r\beta 1}}{dt} &= \tfrac{-1}{R_{r1}(1+\sigma_{s1})} v_{s\beta 1} + \tfrac{\omega_e T_{r1}}{1+\sigma_{r1}} i_{s\alpha 1} \\
&\quad + \tfrac{T_{r1}}{T_{s1}(1+\sigma_{r1})} i_{s\beta 1} + \omega_e T_{r1} i_{r\alpha 1} - i_{r\beta 1} \\
\sigma_2 T_{r2} \tfrac{di_{r\beta 2}}{dt} &= \tfrac{-1}{R_{r2}(1+\sigma_{s2})} v_{s\beta 2} + \tfrac{\omega_e T_{r2}}{1+\sigma_{r2}} i_{s\alpha 2} \\
&\quad + \tfrac{T_{r2}}{T_{s2}(1+\sigma_{r2})} i_{s\beta 2} + \omega_e T_{r2} i_{r\alpha 2} - i_{r\beta 2} \\
J \tfrac{d\omega_e}{dt} &= \tfrac{2}{3}(\tfrac{P}{2})^2 L_o (i_{s\beta 1} i_{r\alpha 1} - i_{s\alpha 1} i_{r\beta 1} - i_{s\beta 2} i_{r\alpha 2} + i_{s\alpha 2} i_{r\beta 2}) \\
&\quad - B\omega_e
\end{aligned}$$

- 9 system states $\Longrightarrow$ $i_{s\alpha 1}$,$i_{s\beta 1}$,$i_{s\alpha 2}$,$i_{s\beta 2}$,$i_{r\alpha 1}$,$i_{r\beta 1}$,$i_{r\alpha 2}$,$i_{r\beta 2}$,ω_e
- Input to the system $\Longrightarrow$ $v_{s\alpha 1}$,$v_{s\beta 1}$,$v_{s\alpha 2}$,$v_{s\beta 2}$

This is the model of two induction machine coupled together. In complete drive system the controller senses or estimates the nine system states and generate voltage inputs to the system.

B. Current controller design

The design of d and q-axis current controller are identical. The switching frequency of the inverter is $5kHz$. Accordingly, the bandwidth is kept at $200Hz$ for current controller. The gain plot of the plant (G_x), PI controller (H_x), open loop transfer function ($G_x H_x$) and closed loop control function (Y_x) are shown in fig–9.

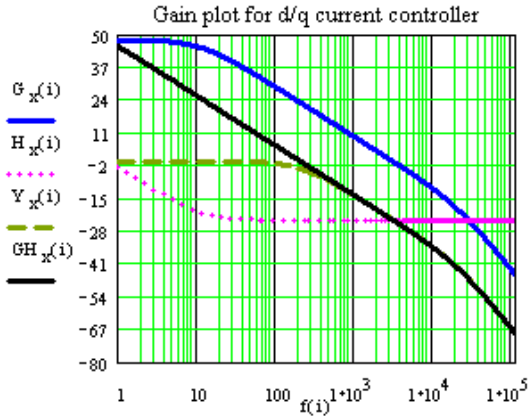

Fig. 9: Gain plot for current controller

C. Flux controller design

The bandwidth of the flux controller is fixed at $6Hz$. The gain plot of the plant (G_f), PI controller (H_f), open loop transfer function ($G_f H_f$) and closed loop control function (Y_f) are shown in fig–10.

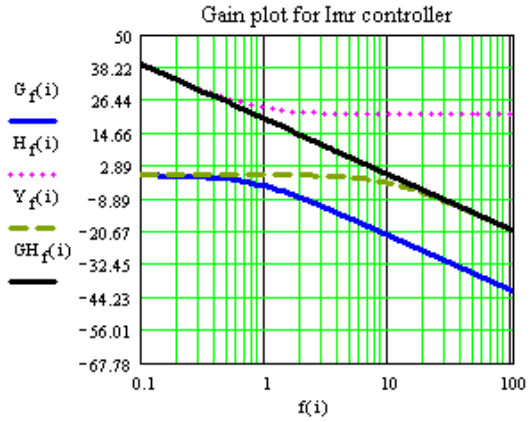

Fig. 10: Gain plot for flux controller

V. Simulation Results

The simulation of the dynamometer system along with v/f drive is carried out and simulation results are shown in fig–11 to fig–19. At t=0 sec, V/f drive is started with no load and a speed command of $25Hz$. At t=0.7 sec, i^*_{mr} command is given for vector controlled drive keeping torque command zero. The torque of $14Nm$ and $-14Nm$ are commanded at t=1.2 sec and t=1.9 sec respectively. The torque command is given with a ramp in order to maintain v/f drive stable.

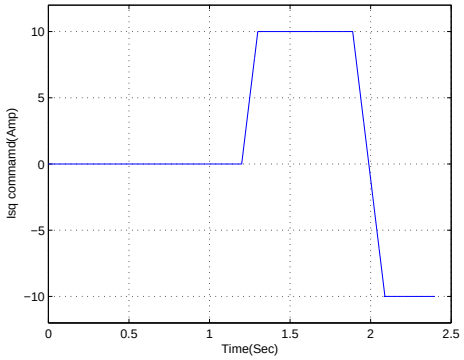

Fig. 11: Isq command

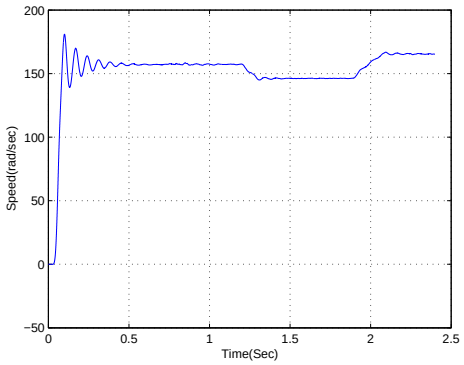

Fig. 12: Speed

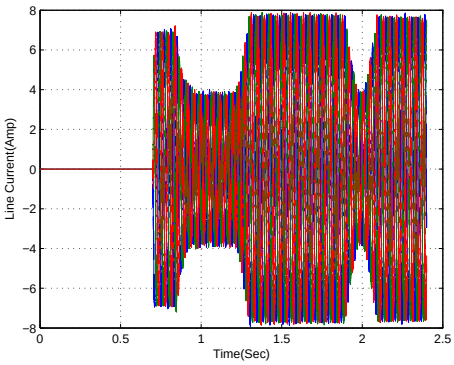

Fig. 13: Line currents

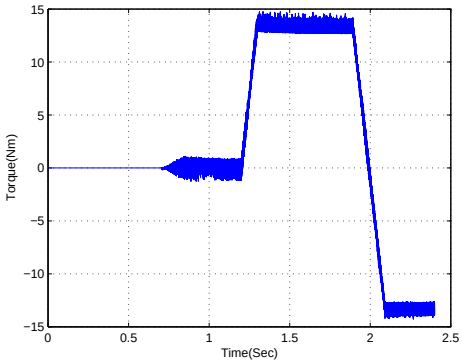

Fig. 14: Torque

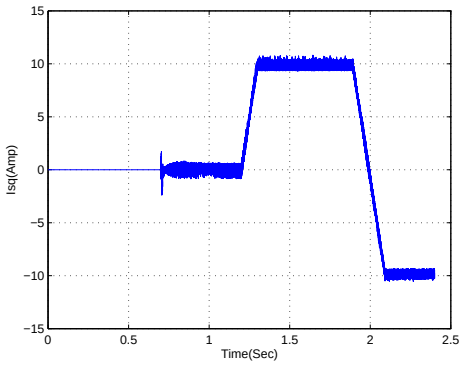

Fig. 15: Isq

VI. Implementation

A. Setup

The experimental setup is shown in fig–20

B. Hysteresis control of DC bus

For a non-electrical system the braking resistor across the DC bus of vector control drive is essential (fig–2). The DC bus is controlled by switching the braking resistor using a hysteresis controller. The hysteresis band is shown fig-21 with $\Delta V = 12V \quad V_{dcref} = 600V \quad V_{dcerror} = V_{dcref} - V_{decaf}$

C. Measured Results

The measured waveforms are furnished in fig–22 to fig–27. Fig–22 shows the I_{mr} buildup at starting of the vector controlled drive on the fly and corresponding R-phase line current. The decoupling between d and q axis quantities is verified through fig–23. Fig–24 shows the change in speed with torque transition. The transient responses of line currents with speed and torque command reversal are given in fig–25 and fig–26 respectively. At near zero speed, an oscillation is observed in speed response because of poor estimation of rotor

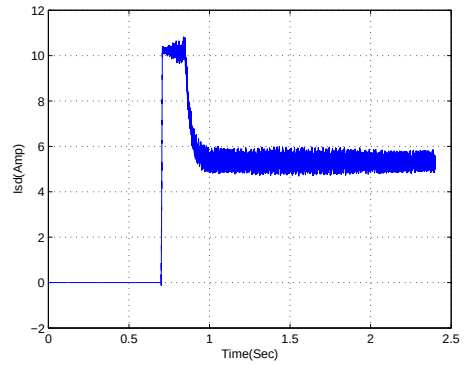

Fig. 16: Isd

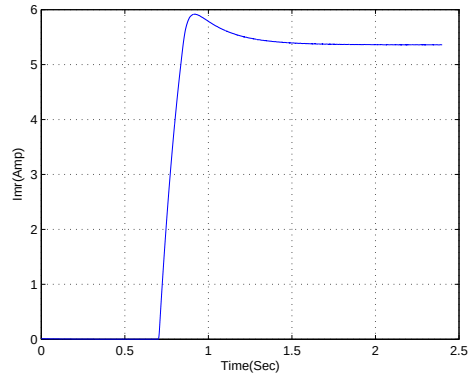

Fig. 17: Imr

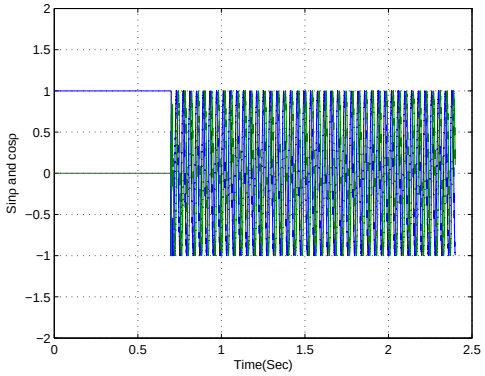

Fig. 18: $cos\rho$ and $sin\rho$

flux position. Fig–27 gives the waveform of DC bus voltage while controlled in hysteresis manner in AC mode.

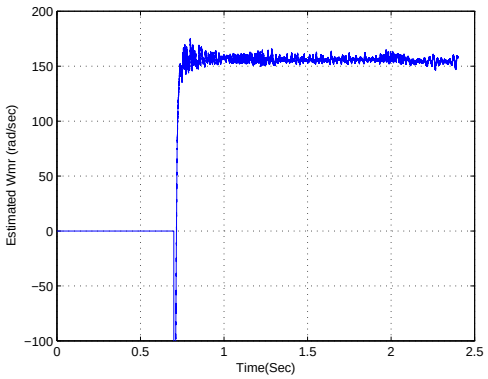

Fig. 19: Estimated ω_{mr}

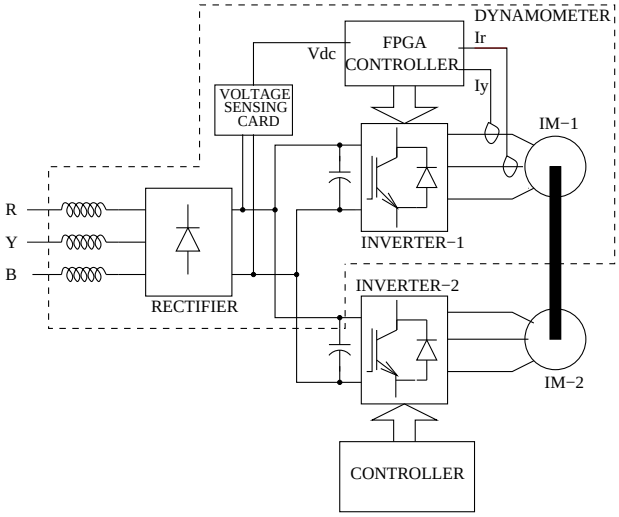

Fig. 20: Experimental Setup

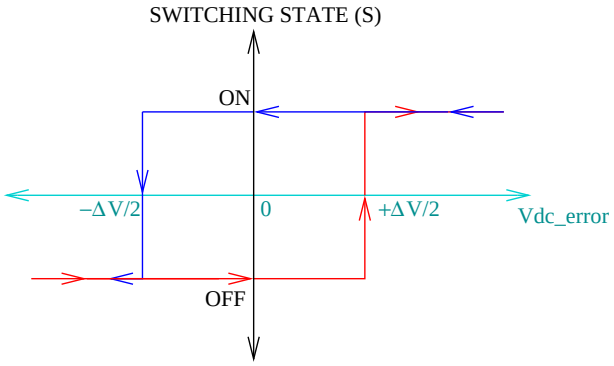

Fig. 21: Hysteresis control

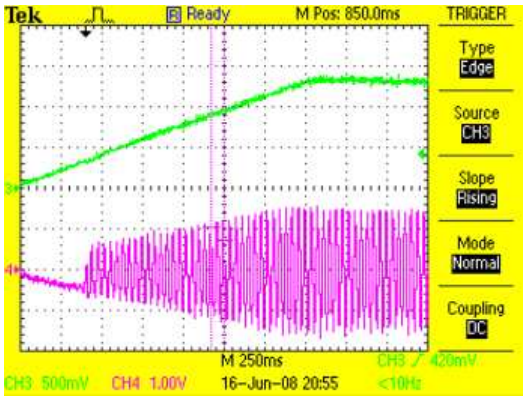

Fig. 22: Imr buildup at starting and Line currents

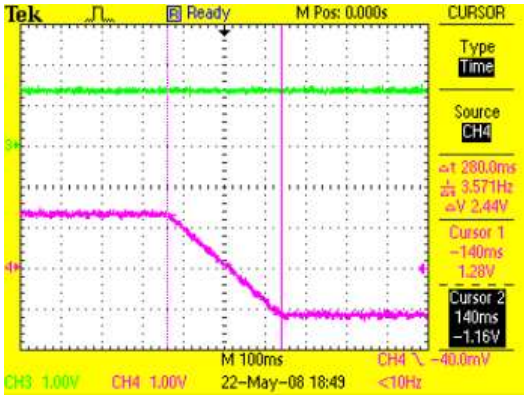

Fig. 23: Steady Imr with torque transition

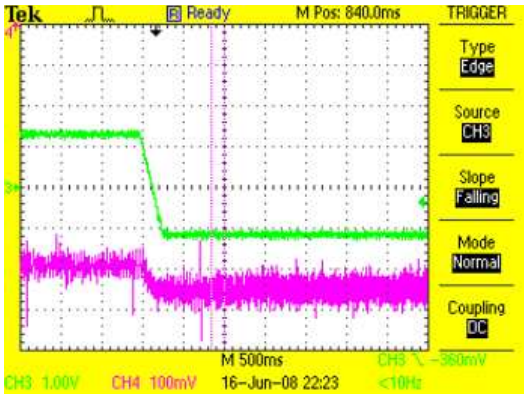

Fig. 24: speed with torque transition

VII. Conclusion

A vector controlled drive has been adopted with suitable changes (load cell) to an induction machine to realize a dynamometer. The dynamometer is capable of loading the system under test in both driving and braking mode. The system can regeneratively load typical v/f machine or other variable speed electrical drives. This will result in lower testing cost in case of large drives. This system may be adopted with suitable modifications to test regenerative UPS, batteries etc.

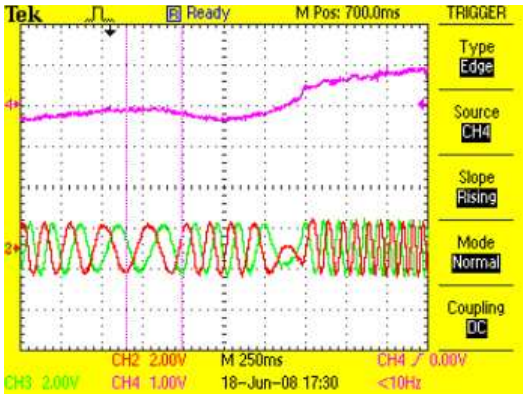

Fig. 25: Line currents with speed reversal

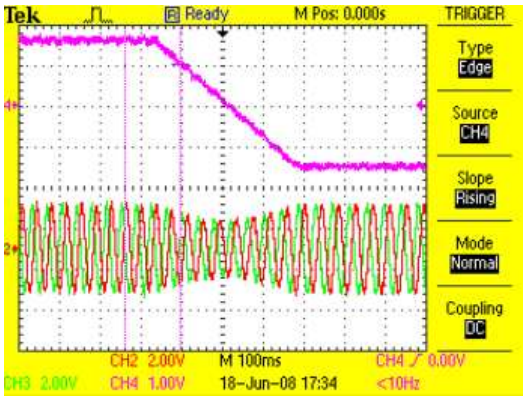

Fig. 26: Line current with torque reversal

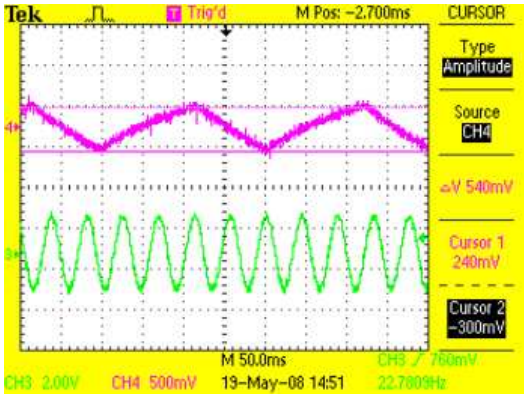

Fig. 27: Hysteresis control of DC bus and line current

References

[1] E. R. Collins, Y. Huang, *A Programmable Dynamometer for Testing Rotating Machinery*, IEEE Transaction on Energy Conversion, vol 9, No 3, September 1994

[2] C. D. Gilberto, D. R. Errera, *A High Performance Dynamometer for Drive System Testing*, Industrial Electronics, Control and Instrumentation, IECON 1997

[3] A. Wallance, A. Jouanne, T. Rollman, *A Fully Regenerative, High Power Testing Facility for Motor, Drives and Generators*, Electric Machines and Drives Conference Record, IEEE International, 1997

[4] W. Leonhard, *Control of Electric Drive*, 3^{rd} Edition, Springer, 2003

[5] B. K. Bose, *Modern Power Electronics and AC Drives*, Prentice Hall, 2005